Available online at www.sciencedirect.com

ScienceDirect

Procedia Engineering 213 (2018) 335–345

Procedia Engineering

www.elsevier.com/locate/procedia

7th International Conference on Fatigue Design, Fatigue Design 2017, 29-30 November 2017, Senlis, France

In-situ crack propagation measurement of high-strength steels including overload effects

David Simunek[a]*, Martin Leitner[a], Florian Grün[a]

[a]*Montanuniversität Leoben, Chair of Mechanical Engineering, 8700 Leoben, Austria*

Abstract

In general, the requirements of endurable light-weight structures are challenging tasks for engineers. High-strength steels provide a major potential by replacing commonly applied construction mild steels. However, a higher notch sensitivity and increased crack propagation rates may decrease the benefit of high-strength steels and their practicability of application. Therefore, reliable assessment methods are demanded to assess fatigue life and crack propagation of welded as well as un-welded structures. For this purpose, an optical measurement system consisting of an industrial camera, telecentric lenses, and special LED components is set-up to analyze crack initiation and propagation of high-strength steels compared to common construction mild steels. Furthermore, an image processing program is developed to investigate the crack length during testing automatically. Indirect potential drop measurement method with crack gauge and optical-light microscopical investigations are utilized to calibrate the elaborated image measurement system. Constant amplitude tests including overloads are performed for high-strength and common construction mild steel specimens to specify the material's service strength. Based on the researched data, material parameters for crack propagation analysis are evaluated for these steel grades.

Peer-review under responsibility of the scientific committee of the 7th International Conference on Fatigue Design.

Keywords: Crack measurement; Optical measurement, Crack propagation; Overload effects; High-strength steel

* Corresponding author. Tel.: +43-(0)3842-402-1452; fax.: +43-(0)3842-402-1402
E-mail address: david.simunek@unileoben.ac.at

1877-7058
Peer-review under responsibility of the scientific committee of the 7th International Conference on Fatigue Design.
10.1016/j.proeng.2018.02.034

1. Introduction

High-strength steel application for light-weight design is a common method to reduce weight and improve fatigue strength of structures. However, a higher notch sensitivity and increased crack growth rates may reduce the benefit of high-strength steel materials. In [1–3] fatigue strength of welded and un-welded base material mild and high-strength steel sheet specimens are investigated. Focus is laid on welded specimens with different weld toe stress concentration factors and the benefits of utilizing high-strength materials. Attention must be drawn on notches and imperfections, which lead to massive reduction on fatigue strength. In this work experimental fatigue crack growth testing is performed on common construction mild steel as well as on high-strength steel sheets. Proper assessment of both crack initiation and propagation stage is of particular interest during testing and subsequent evaluation. To this purpose two different crack growth measurement methods are applied and compared to determine surface crack initiation and propagation length. An optical measurement system consisting of an industrial high-resolution camera, a set of telecentric lenses and a high performance LED-illumination is calibrated for further crack propagation investigation. For image acquisition, the test machine is stopped between a defined number of load-cycles to obtain high accuracy of crack length measurement. The start-up phase and first measurements are given in detail in [4]. In [5,6] similar optical measurement systems are set up for flat test and round bar specimens and have been approved successfully. This paper additionally contributes with an indirect potential drop method to calibrate the optical measurement system. Constant amplitude (CA) loading as well as overload (OL) tests are executed for both material grades. Crack initiation and propagation are separately investigated to draw conclusion from different stages of fatigue life. Overload tests are performed by application of one single OL at a long-crack length of a_{OL} = 8.5 mm. Delayed crack growth retardation is observed and leads to an extension of remaining service life for both types of materials. In [7–12] similar investigations of CA loading and variable amplitude loading were performed on different materials enabling a direct comparison of the presented results.

Nomenclature

a_N	Depth of start notch
a_{OL}	Crack length at overload
a_s	Start crack length
CA	Constant amplitude
C_P	Crack growth rate coefficient according to Paris
K_{max}	Maximum stress intensity factor
m_P	Crack growth rate exponent according to Paris
N_{CA}	Number of load-cycles at constant amplitude loading
N_{Ci}	Number of load-cycles until crack initiation
N_D	Number of delay cycles
N_{DI}	Number of real delay cycles
N_{rout}	Number of run-out load-cycles
OL	Overload
R_{OL}	Overload ratio
$r_p(\varphi)$	Size of the plastic zone
$r_{p,OL}$	Size of the plastic zone at overload (φ=0)
R_σ	Stress ratio
Δa	Crack extension
ΔK	Stress intensity factor range
$\Delta\sigma$	Stress range
ν	Poisson's ratio
σ_y	Yield strength

2. Measurement systems

One aim of the work is the comparison of two different crack growth measurement systems. Therefore, an optical and an indirect potential drop method are applied at several experimental crack propagation samples. This crack growth testing is performed at an electromagnetic resonance test rig.

2.1. Optical measurement

Optical systems are an efficient and reliable method for surface crack detection and crack length measurement. In this work a specialized system with an industrial camera and a telecentric lens is set-up for fatigue crack growth measurement. Adjustable linear bearings and tilt units are utilized to ensure an optimal as well as reproducible, positioning of the camera system. The adjustable optical crack length measurement system is shown in Fig. 1. A high resolution and object field is required wherefore a monochrome five Mega-Pixel camera is chosen [13]. A telecentric lens with a reproduction scale of $\beta = 0.394$, a field depth of $d_f = 2.6$ mm, and an object field of approximately 22x16.5 mm is applied [14]. Although flat specimens are analyzed in this work, one important requirement is a high field depth value to investigate crack propagation at round bar specimens. Due the curved surface of round bars, measurement of crack length is a challenging task and needs a high depth of field value. For that purpose a low opening diameter of the aperture can be recommended, which leads to a long exposure time and requires a strong illumination of the object field. A LED bar is chosen for a diffuse illumination of the polished specimen surface. For a reliable crack length measurement a dark field illumination generally works best. Therefore, the LED bar is mounted in tilted position close to the specimen. In case of a crack, light is reflected to the camera and the surface heterogeneity can be detected. Telecentric lenses have crucial advantages at measurement tasks compared to entocentric lenses. The reproduction scale at entocentric lenses is changing with object distance. Objects, which are localized closer to the lens are depicted with different size; in comparison, telecentric lenses exhibit a constant reproduction scale due to a parallel optical path. [15–17]

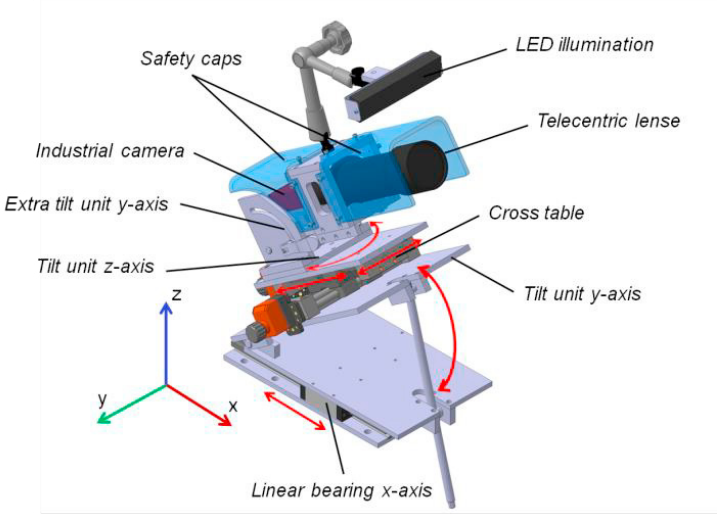

Fig. 1 Adjustable optical crack length measurement system

2.2. Indirect potential drop method

Indirect potential drop method is an universal applicable technique to measure crack propagation at electrically conductive or non-conductive materials. In comparison to the direct potential drop method only surface crack growth can be evaluated. A crack gauge is applied on the specimen surface and the crack length can be continuously measured during testing. The constant current is passed through the gauge and similar to direct potential drop, the resistance based voltage drop is measured. The crack gauge tears equally to the surface crack of the specimen, which leads to an increase of electrical resistance and electric potential. A measuring system by [18] with a precision voltmeter is incorporated. The measurement system is linked to the test machine to record crack length and number of load-cycles simultaneously. The measurement setting and test machine is illustrated in Fig. 2.

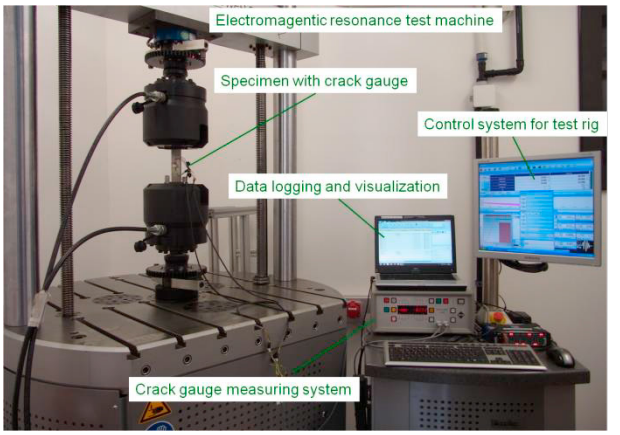

Fig. 2 Test machine with crack gauge measurement system

3. Experimental investigations

The investigated samples are grinded flat, single edge notch tension (SENT) specimens made of both common construction mild steel S355 and high-strength steel S960. The depth of the initial spark eroded start notch is $a_N = 5$ mm (Fig. 3). The evaluation of crack growth rate is performed according to ASTM 647 [19] with a consideration of the geometry factor for stress intensity factor determination based on [20].

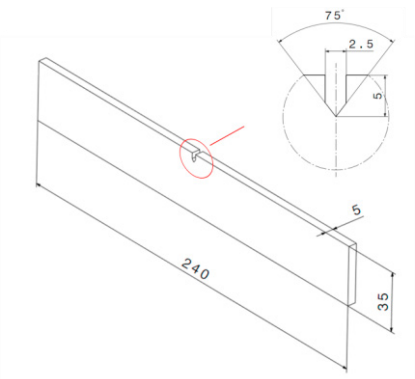

Fig. 3 Specimen geometry with V-notch

Application of crack gauges needs no additional surface treatment and is therefore directly performed with an overlapping of the start notch. Aside, measurement of the crack length by optical system enforces a special treatment of the surface. Hence, the interested region is polished on the opposite side of the applied crack gauge. Before cyclic testing, the crack gauge needs to be pre-cut in the notch root and the measured crack length is considered as an offset value.

3.1. Validation of optical crack growth measurement system

At first, the camera system (Fig. 1) is positioned perpendicular to the surface of the specimen. The operation distance of the telecentric lens is 190 mm. Flat specimens of S355 and S960 are used to compare optical and crack gauge measurement results.

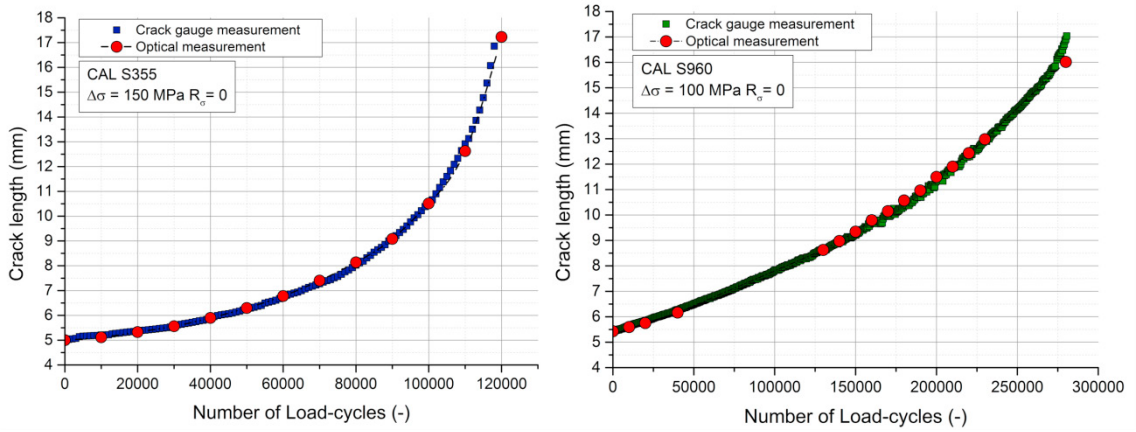

Fig. 4 Comparison of crack length by optical and crack gauge measurement

For crack length monitoring utilizing the optical system, the test machine is periodically stopped to achieve optimal quality of the images. Fig. 4 depicts the comparison of crack gauge and optical measurement for a specimen made of S355 and S960 at constant amplitude loading. The results of the optical measurement are in sound accordance to the crack gauge measurements. The measurement methods are performed on opposite sides of the specimen and thus minor deviations are observed at some measurement points due a slightly asymmetric crack length. Fig. 5 presents two images of optical crack length measurement. Note that the start point of crack length measurement is the notch root. Hence, the length of notch depth has to be added to the total measured length.

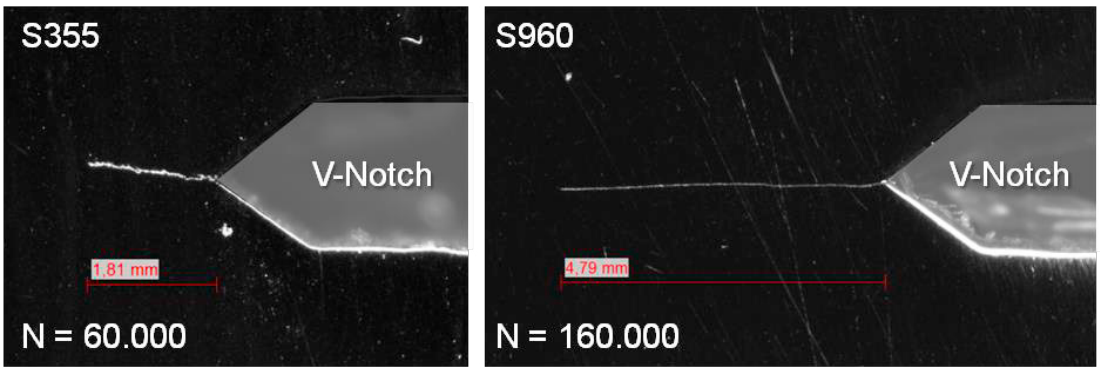

Fig. 5 Optical crack length measurement for S355 and S960 specimen with crack initiation starting from V-notch

3.2. Constant amplitude (CA) tests

Constant amplitude (CA) tests are performed for common construction mild steel S355 and high-strength steel S960. The crack initiation was performed at the same level equal to crack growth testing to investigate the cyclic behavior of these materials at the different propagation stages. Whereas crack initiation at the high-strength material took an increased time compared to the common construction steel, crack growth showed a contrary behavior. Fig. 6 compares the results of the crack growth tests with a nominal stress range of $\Delta\sigma = 62.5$ MPa at a load stress ratio $R_\sigma = 0.1$. The experiments are evaluated after crack initiation at $a_s = 6$ mm, which corresponds to a crack length from the notch tip of $\Delta a = 1$mm.

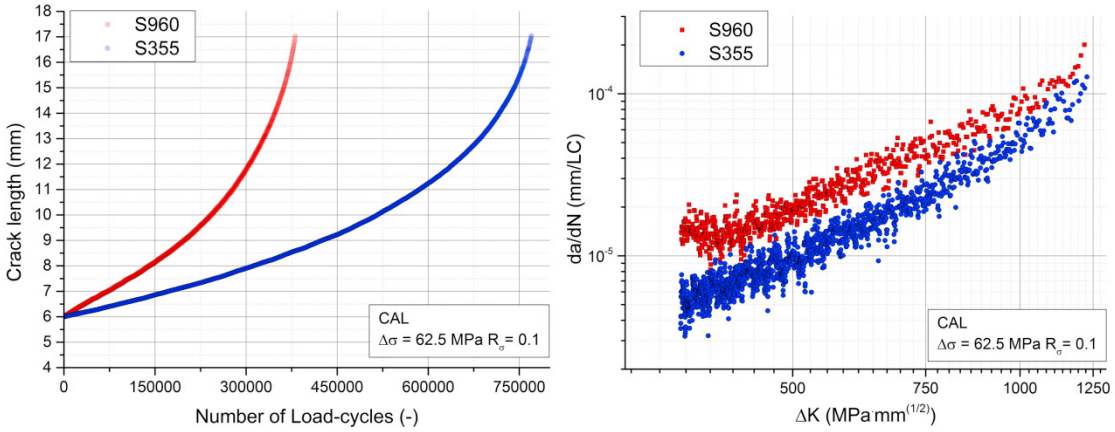

Fig. 6 Crack growth test results for common construction mild steel and high-strength steel

As expected, the evaluation reveals a higher crack propagation rate in case of the high-strength steel S960. Although crack initiation takes significantly longer for the high-strength steel specimens, the crack growth rate indicates increased values compared to the common construction mild steel samples. Investigations of the average load-cycles show an approximately 9.4 times longer crack initiation stage (crack initiation from notch up to $\Delta a = 0.2$ mm) for S960 compared to mild steel S355 (Tab. 1). In some cases even no crack initiation occurred up to a run-out level of $N_{rout} = 5 \cdot 10^7$ load-cycles for high strength steel S960 at the load-level of $\Delta\sigma = 62.5$ MPa.

Load-level $\Delta\sigma$=62.5 MPa	S355	S960
Load-cycles until crack initiation	198,000	1,863,000

Tab. 1 Summary of tested specimens

Evaluated crack propagation parameters according to Paris [21] for both materials are summarized in Tab. 2. Whereas the parameter C_p for S960 is significantly higher, a lower slope m_p is observed compared to S355 for the stable region of the crack growth diagram.

Paris crack growth parameters	S355	S960
C_P (ΔK (MPa$\sqrt{}$mm); da/dN (mm/cycle))	$1.67\ 10^{-12}$	$4.71\ 10^{-11}$
m_P (-)	2.51	2.09

Tab. 2 Evaluated crack propagation parameters

3.3. Overload tests

In general, crack propagation can be significantly affected by overloads (OL). Constant amplitude tests at a nominal stress range of $\Delta\sigma = 62.5$ MPa and a tumescent load stress ratio of $R_\sigma = 0.1$ are performed, but interrupted by a single overload at a crack length $a_{OL} = 8.5$ mm. The applied overload ratio of $R_{OL} = 2.0$ (see Equ. 1) causes a retardation of crack growth rate and leads to a distinctive influence of remaining service life. These investigations are basically performed identical to the CAL-tests for high-strength steel S960 and construction mild steel S355. Fig. 7 shows the evaluation of two investigated S355 specimens. Crack growth rate is accelerated for a few load-cycles after the single overload, followed by an intense retardation. Similar behavior for an austenitic CrNi-steel is observed in [9] and theories to explain this phenomenon are provided.

$$R_{OL} = \frac{K_{max,OL}}{K_{max,BL}} \qquad \text{Equ. 1}$$

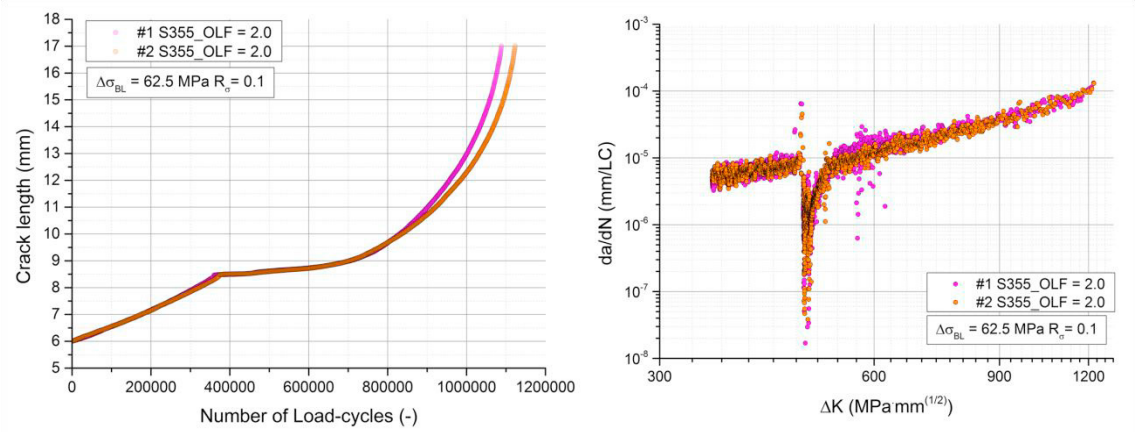

Fig. 7 Crack growth retardation at two S355 specimens after one single overload

The experimental OL-tests for S960 are executed at a higher nominal stress range of $\Delta\sigma = 122.25$ MPa to achieve reliable crack initiation, the overload factor $R_{OL} = 2.0$ is chosen in accordance to the S355 tests. Similarly to the experimental investigations of S355, the crack growth rate increases for some load-cycles after the introduced overload, followed by crack growth retardation. Fig. 8 illustrates the experimental investigations of the overload on crack propagation for the high-strength steel S960.

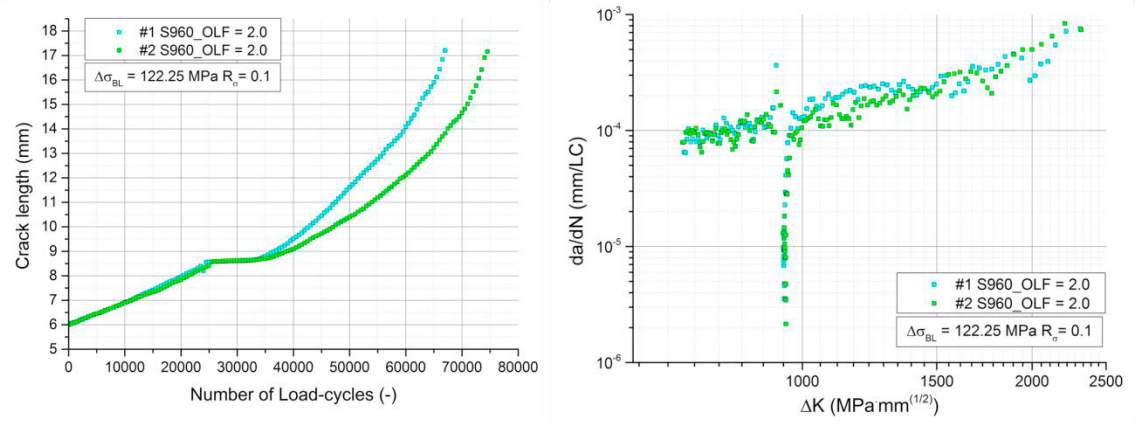

Fig. 8 Crack growth retardation for two S960 specimens after one single overload

In [7,8,22] suggestions for quantification of the retardation effect are given. Based on their work, crack growth retardation is analyzed within these tests. Fig. 9 provides an overview of the delayed cycles after the overload compared to the CA-tests. The results are summarized in Tab. 3 and show an intense influence on crack growth rate after overloading.

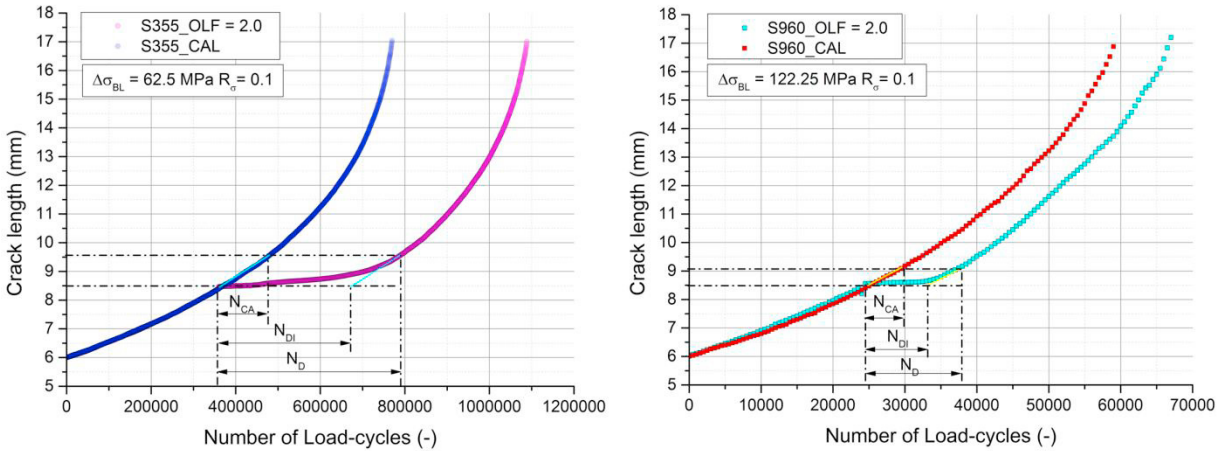

Fig. 9 Comparison of CA-tests and OL-tests for S355 and S960

Although for mild steel S355 and high-strength steel S960 the effect of an overload is clearly distinctive, S355 exhibits an enhanced retardation of the crack growth rate. This may be justified due to a greater plastic zone compared to high-strength steel. According to Equ. 2 [23], the mild steel S355 exhibits a 1.9 times larger plastic zone ($r_{p,OL}$ = 1.440 mm for plane stress) compared to the high-strength steel material ($r_{p,OL}$ = 0.754 mm for plane stress).

$$r_p(\varphi) = \frac{1}{2\pi} \cdot \left(\frac{K_{max}}{\sigma_y}\right)^2 \cdot cos^2\frac{\varphi}{2} \cdot \begin{cases} \left(3 \cdot sin^2\frac{\varphi}{2} + 1\right) & Plane\ Stress \\ \left(3 \cdot sin^2\frac{\varphi}{2} + (1-2\nu)^2\right) & Plane\ Strain \end{cases} \quad \text{Equ. 2}$$

The comparison of remaining service life and number of delay cycles for both materials are summarized in Tab. 3. Due to the single tensile overload a significant influence on the total lifetime is observed, especially for the comparably ductile mild steel S355.

	S355	S960
$N_{CAL\ final}$	770,000	59,000
$N_{OL\ final}$	1,088,500	67,000
$N_{OL\ final}/N_{CAL\ final}$	1.41	1.14
N_D	426,000	13,500
N_{CA}	109,000	4,500
N_{DI}	317,000	9,000

Tab. 3 Summary of experimental results for S355 and S960 specimens

4. Discussion

Crack growth is influenced by residual stresses introduced from manufacturing processes such as rolling, or by additional surface treatments like grinding or polishing, and finally the effective mean stress state is affected in terms of clamping induced bending stresses. Minor deviations of measured crack length are observed at microscopical investigations of final fracture surfaces, see Fig. 10. No correlation between deviation of crack length and surface treatment is observed in this study. The polished surface indicates no detectable influence on crack propagation. Due to flat grinding of the specimens, no fundamental distortion of the sheets occurs. Residual stress and distortion measurements are scheduled for further investigations to determine possible reasons of measured crack length deviations.

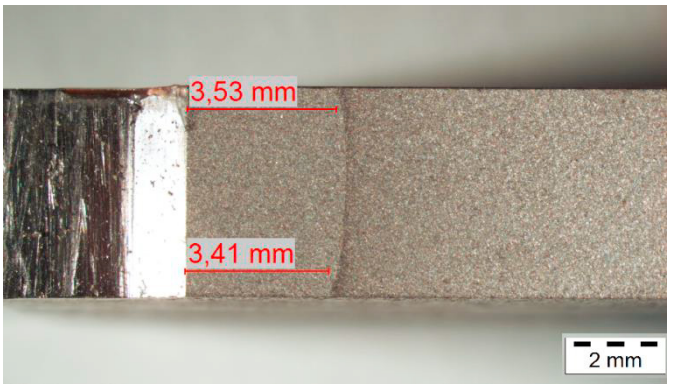

Fig. 10 Deviation of crack length on opposite sides of specimen

Whereas crack propagation for high-strength steel S960 is significantly higher compared to common construction mild steel S355 (both materials tested at same stress level), crack initiation took fundamentally longer (Fig. 11) or in some cases even did not occur. The benefit of high-strength steel application is therefore feasible as long as the crack initiation phase is dominant and no fatigue crack is initiated. This behavior makes a specification of inspection intervals necessary due to the remaining risk of crack initiation and subsequent comparably fast propagation rate for high-strength steels.

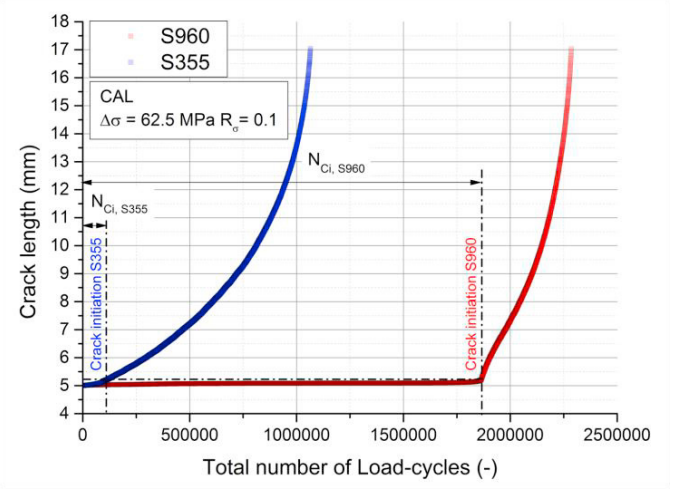

Fig. 11 Comparison of crack initiation and crack growth

5. Conclusions

The demand of high-strength steel for light-weight structures requires a sophisticated investigation of crack initiation and crack growth. To this purpose an optical crack length measurement system is set-up and successfully calibrated. Additionally, an indirect potential drop method is applied for continuously crack length measurement during testing. Constant amplitude as well as overload tests are performed to examine crack growth behavior for common construction mild steel S355 and high-strength steel S960. Crack growth parameters are properly determined and compared for these steel grades. The remaining service life due to one single overload is strongly influenced, whereat the common construction steel possesses a more pronounced retardation effect due to a 1.9 times greater plastic zone compared to the high-strength steel. The overload leads to 1.41 and 1.14 times longer crack growth stage compared to CA-tests for S355 and S960 respectively. The crack growth rate is approximately 300 times ($9 \cdot 10^{-6}$ to $3 \cdot 10^{-8}$ mm/cycle) reduced right after the overload at common construction mild steel, whereas crack propagation at the high-strength steel is decreased about 50 times ($1.5 \cdot 10^{-4}$ to $3 \cdot 10^{-6}$ mm/cycle). Although the high-strength steel S960 exhibits faster crack growth, crack initiation requires 9.4 times longer compared to the common construction steel S355 at the same load-level. Further investigations considering crack initiation and crack growth at constant amplitude loading as well as variable amplitude loading for mild and high-strength steel grades are scheduled to differentiate the effects on varying crack propagation stages. Influence of bending stresses due to distortion and residual stresses may affect asymmetric crack extension. Hence, distortion measurements and strain gauge based surface stress analysis during clamping and testing are of interest. Finally, residual stress distribution within the surface layer will be determined by X-ray diffraction analysis.

Acknowledgements

Financial support by the Austrian Federal Government (in particular from Bundesministerium für Verkehr, Innovation und Technologie and Bundesministerium für Wissenschaft, Forschung und Wirtschaft) represented by Österreichische Forschungsförderungsgesellschaft mbH and the Styrian and the Tyrolean Provincial Government, represented by Steirische Wirtschaftsförderungsgesellschaft mbH and Standortagentur Tirol, within the framework of the COMET Funding Programme is gratefully acknowledged.

References

[1] M. Leitner, M. Stoschka, W. Eichlseder, Fatigue enhancement of thin-walled, high-strength steel joints by high-frequency mechanical impact treatment, Weld World 58 (1) (2014) 29–39.
[2] M. Leitner, M. Stoschka, M. Ottersböck, D. Simunek, Ermüdungsfestigkeit hochfester Stahlschweißverbindungen, Berg Huettenmaenn Monatsh 160 (1) (2015) 9–14.
[3] M. Leitner, M. Stoschka, Influence of steel grade on the fatigue strength enhancement by high frequency peening technology on longitudinal fillet weld gusset, in: Journal of Engineering and Technology, pp. 80–90.
[4] A.R. Lintner, Aufbau eines optischen Systems zur Rissfortschrittsmessung an Flachproben, Leoben, 2017.
[5] T. Thurner, Real-Time Detection and Measurement of Cracks in Fatigue Test Applications, 1st ed., Springer US, Berlin, 2015.
[6] B. Lian, A. Ueno, T. Iwashita, Development of in-situ fatigue crack observing system for rotating bending fatigue testing machine, Frattura ed Integrità Strutturale (35) (2016) 389–395.
[7] M. Skorupa, Load interaction effects during fatigue crack growth under variable amplitude loading-A literature review. Part I: Empirical trends, Fatigue & Fracture of Engineering Materials & Structures (21) (1998) 987–1006.
[8] M. Sander, H.A. Richard, Fatigue crack growth under variable amplitude loading Part I: experimental investigations, Fat Frac Eng Mat Struct 29 (4) (2006) 291–301.
[9] C. Bichler, R. Pippan, Effect of single overloads in ductile metals: A reconsideration, Engineering Fracture Mechanics 74 (8) (2007) 1344–1359.
[10] J. Schijve, Fatigue crack growth in the aluminium alloy D16 under constant and variable amplitude loading, International Journal of Fatigue 26 (1) (2004) 1–15.
[11] Z. Ding, X. Wang, Z. Gao, S. Bao, An experimental investigation and prediction of fatigue crack growth under overload/underload in Q345R steel, International Journal of Fatigue 98 (2017) 155–166.

[12] D. Simunek, M. Leitner, J. Maierhofer, H.-P. Gänser, Fatigue Crack Growth Under Constant and Variable Amplitude Loading at Semi-elliptical and V-notched Steel Specimens, Procedia Engineering 133 (2015) 348–361.
[13] Allied Vision Technologies GmbH, Manta G-505, available at https://www.alliedvision.com/de/produkte/kameras/kameradetails/Manta/G-505.html (accessed on July 4, 2017).
[14] Sill Optics GmbH & Co. KG, Telecentric Lenses - Product overview, available at http://www.silloptics.de/1/products/machine-vision/telecentric-lenses/product-overview/ (accessed on July 4, 2017).
[15] Vision Doctor, Telecentric Lenses, available at http://www.vision-doctor.com/en/telecentric-lenses.html (accessed on July 4, 2017).
[16] Stemmer Imaging, Das Handbuch der Bildverarbeitung, Stemmer Imaging, Puchheim, 2013.
[17] Opto Engineering, Telecentric lenses tutorial: Basic information and working principles, available at http://www.opto-engineering.com/resources/telecentric-lenses-tutorial (accessed on July 4, 2017).
[18] Russenberger Prüfmaschinen AG, available at http://www.rumul.ch/250_products.php (accessed on July 4, 2017).
[19] ASTM International, Standard Test Method for Measurement of Fatigue Crack Growth Rates, West Conshohocken, PA, 2000, available at https://www.astm.org/DATABASE.CART/HISTORICAL/E647-00.htm (accessed on July 4, 2017).
[20] H. Tada, P.C. Paris, G.R. Irwin, The Stress Analysis of Cracks Handbook, Third Edition, ASME, Three Park Avenue New York, NY 10016-5990, 2000.
[21] P.C. Paris, F. Erdogan, A critical analysis of crack propagation laws, Journal Basic Engineering (85) (1963) 528–534.
[22] H.A. Richard, M. Sander, Ermüdungsrisse: Erkennen, sicher beurteilen, vermeiden, 2nd ed., Vieweg+Teubner Verlag, Wiesbaden, 2012.
[23] D. Gross, T. Seelig, Bruchmechanik: Mit einer Einführung in die Mikromechanik, 4th ed., Springer, Berlin, 2007.